Research Article | Vol. 26, No. 4 | 19 Feb 2018 | OPTICS EXPRESS 4631
Optics EXPRESS

Maximizing the field of view and accuracy in 3D Single Molecule Localization Microscopy

SOHAIB ABDUL REHMAN,[1]* ALEXANDER R. CARR,[2] MARTIN O. LENZ,[1] STEVEN F. LEE,[2] AND KEVIN O'HOLLERAN[1]

[1]*Cambridge Advanced Imaging Centre, University of Cambridge, Cambridge, CB2 3DY, UK*
[2]*Department of Chemistry, University of Cambridge, Cambridge, CB2 1EW, UK*
[*]*sa753@cam.ac.uk*

Abstract: Super-resolution techniques that localize single molecules in three dimensions through point spread function (PSF) engineering are very sensitive to aberrations and optical alignment. Here we show how double-helix point spread function is affected by such mis-alignment and aberration. Specifically, we demonstrate through simulation and experiment how misplacement of phase masks in infinity corrected systems is a common source of significant loss of accuracy. We also describe an optimal alignment and calibration procedure to correct for these errors. In combination, these optimizations allow for a maximal field of view with high accuracy and precision. Though discussed with reference to double-helix point spread function (DHPSF), the optimization techniques are equally applicable to other engineered PSFs.

OCIS codes: (100.6640) Superresolution; (180.2520) Fluorescence microscopy; (180.6900) Three-dimensional microscopy.

References and links

1. E. Betzig, G. H. Patterson, R. Sougrat, O. W. Lindwasser, S. Olenych, J. S. Bonifacino, M. W. Davidson, J. Lippincott-Schwartz, and H. F. Hess, "Imaging intracellular fluorescent proteins at nanometer resolution," Science **313**, 1642–1645 (2006).
2. M. J. Rust, M. Bates, and X. Zhuang, "Sub-diffraction-limit imaging by stochastic optical reconstruction microscopy (STORM)," Nat. Methods **3**, 793–796 (2006).
3. B. Huang, W. Wang, M. Bates, and X. Zhuang, "Three-dimensional super-resolution imaging by stochastic optical reconstruction microscopy," Science **319**, 810–813 (2008).
4. S. R. P. Pavani, M. A. Thompson, J. S. Biteen, S. J. Lord, N. Liu, R. J. Twieg, R. Piestun, and W. Moerner, "Three-dimensional, single-molecule fluorescence imaging beyond the diffraction limit by using a double-helix point spread function," Proc. Natl. Acad. Sci. **106**, 2995–2999 (2009).
5. A. von Diezmann, Y. Shechtman, and W. Moerner, "Three-dimensional localization of single molecules for super-resolution imaging and single-particle tracking," Chem. Rev. **117**(11), 7244–7275 (2017).
6. S. R. P. Pavani and R. Piestun, "Three dimensional tracking of fluorescent microparticles using a photon-limited double-helix response system," Opt. Express **16**, 22048–22057 (2008).
7. M. Badieirostami, M. D. Lew, M. A. Thompson, and W. Moerner, "Three-dimensional localization precision of the double-helix point spread function versus astigmatism and biplane," Appl. Phys. Lett. **97**, 161103 (2010).
8. M. D. Lew, M. A. Thompson, M. Badieirostami, and W. Moerner, "In vivo three-dimensional superresolution fluorescence tracking using a double-helix point spread function," Proc. SPIE **7571**, 75710Z (2010).
9. A. von Diezmann, M. Y. Lee, M. D. Lew, and W. Moerner, "Correcting field-dependent aberrations with nanoscale accuracy in three-dimensional single-molecule localization microscopy," Optica **2**, 985–993 (2015).
10. B. Shuang, W. Wang, H. Shen, L. J. Tauzin, C. Flatebo, J. Chen, N. A. Moringo, L. D. Bishop, K. F. Kelly, and C. F. Landes, "Generalized recovery algorithm for 3d super-resolution microscopy using rotating point spread functions," Sci. Rep. **6**, 30826 (2016).
11. A. R. Carr, A. Ponjavic, S. Basu, J. McColl, A. M. Santos, S. Davis, E. D. Laue, D. Klenerman, and S. F. Lee, "Three-dimensional super-resolution in eukaryotic cells using the double-helix point spread function," Biophysical J. **112**, 1444–1454 (2017).
12. S. R. P. Pavani and R. Piestun, "High-efficiency rotating point spread functions," Opt. Express **16**, 3484–3489 (2008).
13. M. D. Lew, A. R. von Diezmann, and W. Moerner, "Easy-DHPSF open-source software for three-dimensional localization of single molecules with precision beyond the optical diffraction limit," Protocol Exchange **2013**, 26 (2013).

#315713 https://doi.org/10.1364/OE.26.004631
Journal © 2018 Received 14 Dec 2017; revised 11 Jan 2018; accepted 11 Jan 2018; published 13 Feb 2018

Optics EXPRESS

1. Introduction

Super-resolution microscopy techniques enable the answering of biological questions that require information below the optical diffraction limit of light. Single Molecule Localization Microscopy (SMLM) is a group of super-resolution techniques that resolve the position of individual molecules by separating their fluorescence emissions in time to gain higher spatial information [1,2]. Engineered point spread functions (PSFs) can allow single molecules to be localized in all three spatial dimensions [3–5]. One such engineered PSF is the double-helix point spread function (DHPSF) which can achieve a depth of field of over 3 μm with near uniform localization precision [6]. These techniques are routinely implemented using commercial microscopy platforms with standard infinity corrected optics.

Infinity corrected objective lenses output collimated light rays from point sources in their focal plane, which are then typically focused to the image plane by a tube lens. Due to highly corrected collimation of light rays after the objective, the exact distance between the objective and the tube lens is not crucial for the majority of imaging modalities such as point-scanning techniques or 2D localization microscopy. However, for imaging techniques involving phase-modifying optics the position of the conjugate back focal plane (BFP), relative to the tube lens, becomes critical. In an idealized microscope schematic, it is common to simply show the microscope objective as a lens functioning in a 4f setup (see Fig. 1(a)). The nature of infinity corrected optics invalidates this simple schematic, with the BFP not lying in the focal plane of the tube lens. This has the effect, when relaying the image plane, of separating the conjugate BFP with the Fourier plane of the imaged plane (the plane in which the camera is placed) as shown in Fig. 1(b). For phase-modifying optics in microscopy literature this error is routinely made [4,7–11] with the implication being that the experiment was performed sub-optimally for these techniques.

Specifically for 3D localization microscopy using DHPSF, erroneous placement of phase modifying optics, leads to a loss of accuracy, which is usually avoided by simply restricting imaging to a reduced field of view (FOV) for high NA lenses, which is far from the ideal solution. Here we present a way to maximize the accuracy and hence the usable FOV in DHPSF localization microscopy by minimizing the spatial variance of the DHPSF. We will demonstrate the effects of suboptimal phase mask placement through simulations and experiments as well as describe an alignment procedure to correct and optimize such systems. These optimization techniques, though discussed with reference to DHPSF, due to its large depth of field, are equally relevant to other PSF engineering methods [5].

2. Experimental Setup

A commercial inverted microscope frame (Leica, DMI RE2) was customized for localization microscopy by removing all components from the excitation path. Excitation beam (λ = 638 nm) from a laser combiner (Omicron LightHUB) was collimated (Thorlabs, RC12APC-P01) to a 8 mm diameter and then demagnified onto the sample using 250 mm focal length achromatic doublet (Thorlabs) and silicone oil objective (Olympus, UPLSAPO60xS). Emission signal was collected using the same objective and focused to the image plane using a 200 mm focal length tube lens. A quad band dichroic (Chroma, ZT405/488/561/640rpc) and a wavelength filter (Semrock, BLP01-647R-25) separated excitation and emission light. Relay lens (125 mm focal length) demagnified the back focal plane to match the beam to the phase mask. A lens (125 mm focal length) then imaged the beam onto an sCMOS camera (Hamamatsu, Flash 4.2), as shown in Fig. 1. The DHPSF was generated using commercially available phase mask (Double Helix Optics, USA), optimized for uniform localization precision over a 3 μm depth of field [12].

Optics EXPRESS

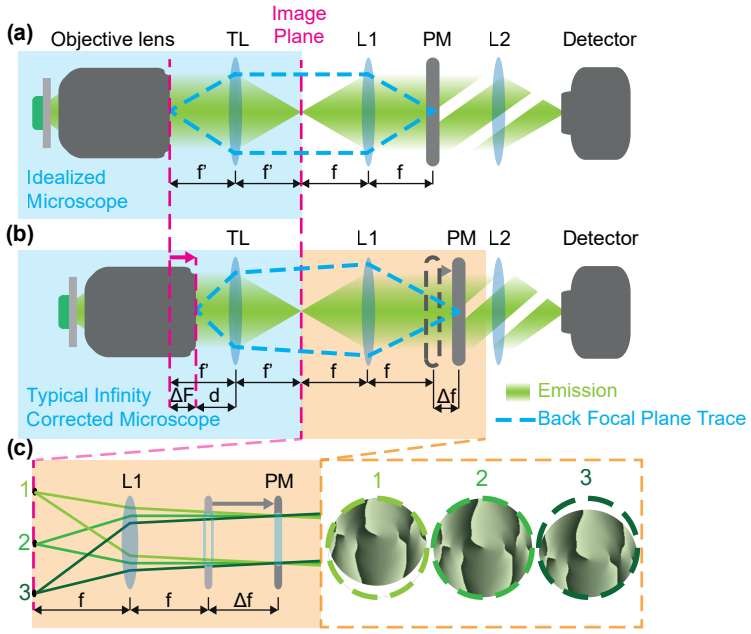

Fig. 1. Emission paths for (a) idealized microscope and (b) typical infinity corrected microscope (note that the position of image plane is unchanged but conjugate BFP shifts). (c) overlap of light beams with the phase mask, from different points in the FOV, when phase mask is displaced from the conjugate BFP. The labels TL, L1, L2 and PM represent tube lens, the first and second lenses of 4f systems and the DHPSF phase mask respectively.

3. Alignment of Phase Mask

The DHPSF encodes the lateral and axial positions of an emitter in the center of its two lobes and the angle between them respectively. In the absence of aberration, the DHPSF rotates about the true position of the emitter, with the rotation angle determined by the emitter's axial position. However, lateral shifts in the position of the DHPSF from the ground truth have been reported [9, 11], which (if not corrected) significantly affect the accuracy of localizations. We found that the major source of this perturbation is the microscope infinity system design shown in Fig. 1(b). This design is advantageous for two-dimensional imaging techniques since the tube lens is positioned to minimize vignetting. The flexible positioning of the tube lens also allows other optics to be installed in infinity space.

For volumetric imaging techniques, infinity corrected optics can introduce significant errors if the exact positioning of the tube lens is not taken into consideration when placing the phase mask. If the phase mask is not placed precisely in the conjugate back focal plane (BFP), off-axis point sources project exit pupils laterally shifted relative to the phase mask (see Fig. 1(c)). The exact perturbation to the DHPSF depends on the size of this lateral shift and the wavefront shape.

For a given microscope setup, the correct position of the conjugate BFP (and the optimal position of the phase mask) can be found by iterative displacement of the phase mask along the optical axis to minimize lateral shifts of point sources (in the imaged volume) as a function of their axial positions. Alternatively, it can be found by sending in a collimated light through the microscope objective, which results in a diffraction limited spot in the conjugate BFP as shown in Fig. 1(b). It is important to note that a change in the excitation wavelength results in a shift in the position of the conjugate BFP. Moreover, phase masks are designed to work optimally for a specific wavelength. Hence, different excitation wavelengths require different phase masks and

Optics EXPRESS

consideration of chromatic aberration.

4. Mathematical Modeling

The electric field in the BFP of the objective is given by the Fourier transform of the field in the focal plane of the objective. Due to incoherent nature of the point sources in the imaged volume, the field in the BFP is given as:

$$E(\mathbf{k}, f_o) \propto \sum_{n=1}^{\mathrm{N}} \mathcal{F}[E(\mathbf{r}, z)]\, O(\mathbf{k}) \tag{1}$$

here, $\mathbf{k} = (k_x, k_y)$ are the normalized coordinates of the BFP of the objective, $E(\mathbf{r}, z)$ and $E(\mathbf{k}, f_o)$ are the fields in the front and the back focal plane of the objective respectively, N is the number of emitting point sources in the imaged volume, f_o is the focal length of the objective and $O(k)$ is the support of the Optical Transfer Function of the system (in most cases a unit circle).

Light from different point sources overlap in the BFP with linear (tilt) and parabolic (defocus) phases depending on their lateral and axial positions respectively. The field at the BFP is relayed via TL and $L1$ (see Fig. 1). If $\mathbf{r}$ represents the lateral position of a point source in the imaged volume, the phase tilt after $L1$, by using the shift property of the Fourier Transform, is given as:

$$\phi(\mathbf{k}) = \exp\left(iM\frac{\mathbf{k}\cdot\mathbf{r}}{f}\right) \tag{2}$$

here, M is the magnification of the microscope and f is the focal length of $L1$. On propagation from the conjugate BFP any linear phase will cause lateral shifts from the optical axis. As such, any axial displacement, Δf, of the phase mask from the conjugate BFP will result in mismatch of the phase mask center with the beam:

$$\Delta\mathbf{k} = M\frac{\mathbf{r}}{f}\Delta f. \tag{3}$$

here, $\Delta\mathbf{k}$ is the lateral shift between the center of the phase mask and the light beam from a point source located at $(\mathbf{r}, \mathbf{z})$. As $\Delta\mathbf{k}$ is a function of $\mathbf{r}$ we can consider the effect in 3D by studying the effect of radial misalignment of the DHPSF phase mask.

It is helpful to describe this misalignment by back-projecting the effect of the phase mask to the conjugate BFP for each $\mathbf{r}$. This virtual BFP now has perfect overlap of all ray bundles but each point source with $|\mathbf{r}| > 0$ *sees* a different, shifted, phase mask. The phase of each source emitted at $(\mathbf{r}, z)$ is modified in the BFP to become:

$$\mathbf{E}_\mathbf{r}(\mathbf{k}, z) = \exp\left[i(\alpha(z)(2k^2 - 1) + \phi_{DH}(\mathbf{k} - \Delta\mathbf{k}))\right] \tag{4}$$

where $\alpha(z)$ is the coefficient of the Zernike defocus term, $(2k^2 - 1)$, the magnitude of which changes with the axial position of a point emitter causing the DHPSF to rotate, $k = |\mathbf{k}|$ and ϕ_{DH} is the phase of the phase mask. For a point source with $|\mathbf{r}| > 0$ and $\alpha(z) \neq 0$, ϕ_{DH} is added on a phase gradient (due to shift between the centers of the wavefront and the phase mask), resulting in laterally displaced DHPSF.

5. Simulations

In order to understand the effect of phase mask displacement from the conjugate BFP, we modeled the shift-varying DHPSF formed by such a positioning. The phase required to generate the DHPSF was obtained from [12]. MATLAB (Mathworks, USA) was used to calculate the images formed from point sources (at $|\mathbf{r}| = 6.5\ \mu$m, $13\ \mu$m and $20\ \mu$m) over a $50 \times 50\ \mu$m area. Images were calculated using Eq. (4) across the depth-of-field of $3\ \mu$m at 300 nm intervals. These parameters

Optics EXPRESS

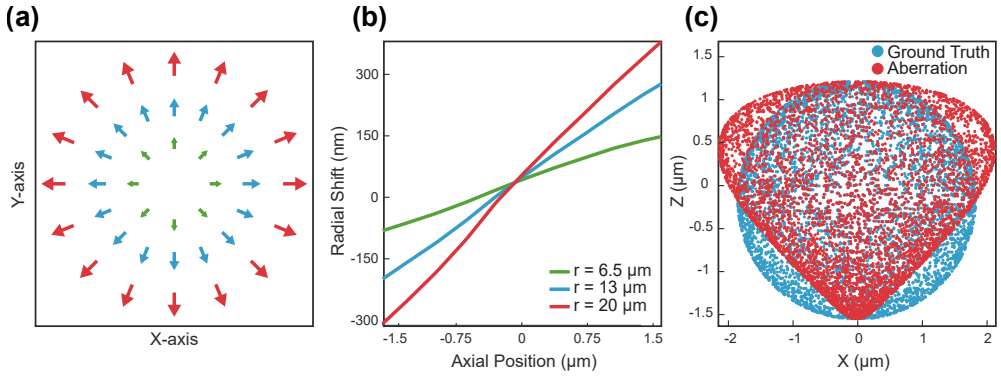

Fig. 2. Simulation results for 35 mm displacement between the phase mask and the conjugate BFP of the objective. (a) shows radial nature of the spatially varying DHPSFs and (b) shows these lateral shifts for three distances from the center of the FOV. (c) depicts distortion in a spherical object due to the radial shifts (errors exaggerated 10 times).

were selected to match simulations to our experimental setup. Finally the images were input into the freely available Easy-DHPSF software [13] for 3D localization. Figure 2(b) shows the results of such a simulation with $\Delta f = 35$ mm (which is the distance between the conjugate BFP and the Fourier plane of the imaged plane in our experimental setup).

The results clearly show the effect of Δf, namely a radial displacement of the DHPSF that grows larger with $\mathbf{r}$. The magnitude and direction (along $\mathbf{r}$) of this radial shift is plotted for three different simulated radii in Fig. 2(b). The displacement is almost linear and the gradient grows quickly with $|\mathbf{r}|$. This displacement is fundamentally a loss of accuracy in localizing the point emitters and can be as much as several hundred nanometers.

To explore the effect of this aberration on three dimensional shapes, we simulated the effect of imaging a spherical object labeled with point emitters on the surface (Fig. 2(c)). The induced accuracy error being linear in axial position (defocus) results in the distortion of a spherical ground truth to a tear drop shape. This shape although idealistic is equivalent to imaging the labeled membrane of a cell.

6. Experimental Results and Discussion

To verify our analysis, we adhered fluorescent beads (Invitrogen, 100 nm) to a cover slip surface using poly-l-lysine (PLL). Experiments were performed by placing the phase mask at different distances from the conjugate BFP of the objective and a 50×50 μm area was imaged. A piezo driven stage (PIFOC, PI) was used to axially scan the sample over a 3 μm distance at 100 nm intervals. A typical FOV contained around 30 beads, whose positions were localized using Easy-DHPSF. The results of these localizations were then used to interpolate across the full FOV. Results of this measurement for three different $|\mathbf{r}|$ (as seen in Fig. 3(a)) and three Δf are shown in Figs. 3(d)-(f).

Results, in accordance with our mathematical analysis and simulations, show that radial shifts are larger for beads away from the center of the FOV and increase as beads are moved out of the focal plane of the objective. Similar lateral shifts have been reported in [9]. When the phase mask is moved closer to the conjugate BFP the radial displacement is reduced, verifying our hypothesis that spatially varying PSF is a consequence of the phase mask being displaced from the conjugate BFP of the objective.

The conjugate BFP contains perfect overlap of emitted light from all beads in the FOV, so PSFs no longer vary spatially. However, due to the extent of uncontrollable system aberrations, a

Optics EXPRESS

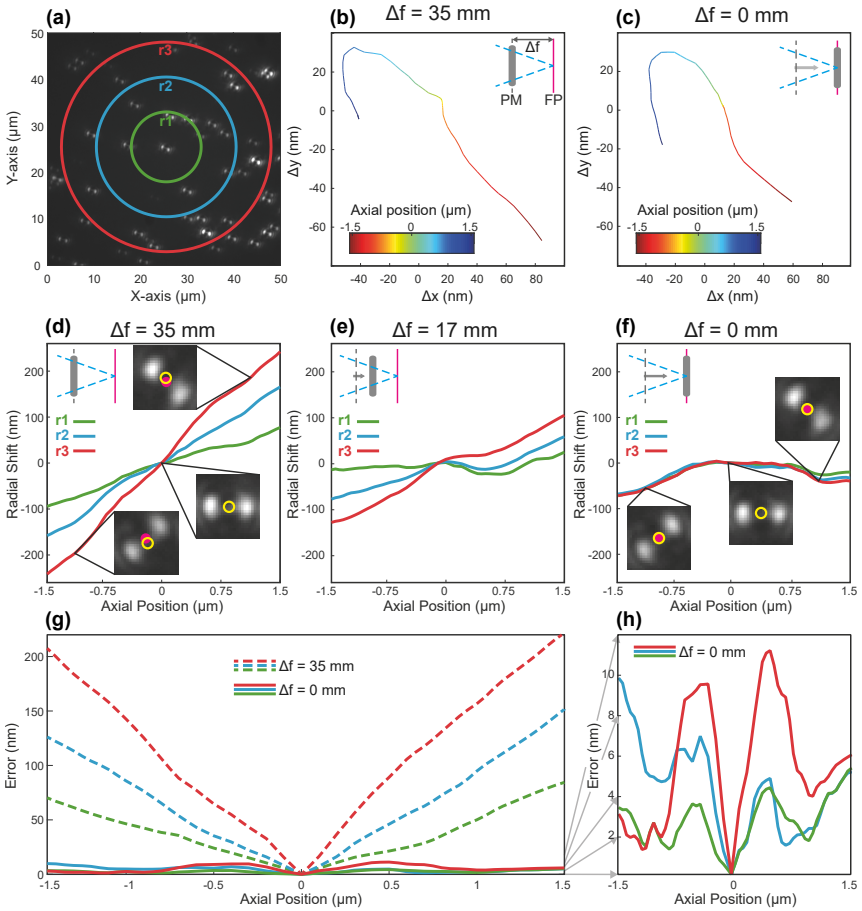

Fig. 3. (a) A representative image showing a distribution of fluorescent beads with three different radii marked at 7 μm, 14 μm and 21 μm. (b) and (c) show the global correction calculated from the average of bead positions assuming a shift-invariant PSF for phase mask displacements of 35 mm and 0 mm. (d), (e) and (f) show the radial shift in bead position when interpolated across the FOV for the three different phase mask displacements of 35 mm, 17 mm and 0 mm from the conjugate BFP. Curves with different colors show shifts at radial distances as shown in (a). (g) and (h) show resulting mean squared error if the global corrections shown in (b) and (c) are simply applied to a shifted phase mask (35 mm) and the correctly positioned phase mask respectively.

global correction is required. We computed this global correction from the average lateral shifts of all beads in the FOV and it is shown in Fig. 3(c). Due to the spatial invariance of the PSF, this correction can also be computed from the lateral shifts of any single bead in the FOV. This allows users to use common algorithms for DHPSF localizations, which assume a shift invariant PSF [13]. After applying the global correction, we achieved accuracy of less than 20 nm over the entire FOV, as shown in Fig. 3(h). Not only is this accuracy in line with precision but the usable FOV is greatly increased. In our experiments the 50×50 μm area was a limitation of our excitation beam diameter and with more uniform illumination we expect high accuracy and precision across the FOV limited by the objective itself.

To demonstrate how erroneous performing a global correction with a misplaced phase mask can be, a global correction for $\Delta f = 35$ mm is shown in Fig. 3(b). Although this appears similar

Optics EXPRESS

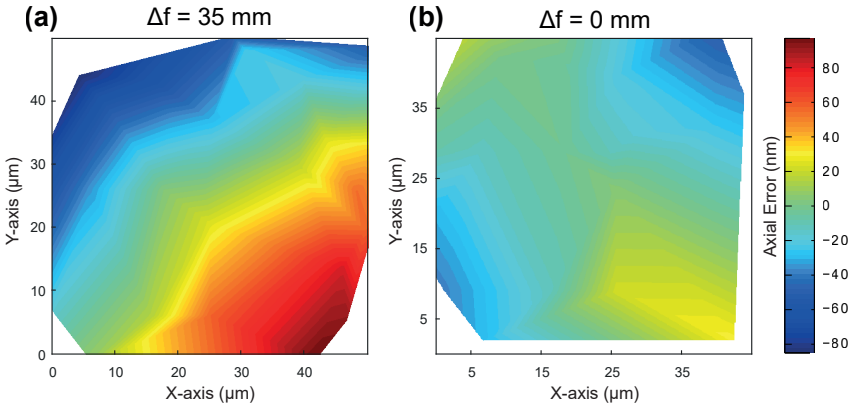

Fig. 4. Maximum axial errors for (a) $\Delta f = 35$ mm and (b) $\Delta f = 0$ mm.

to the correction in Fig. 3(c) it results in an order of magnitude increase in errors, as seen in Fig. 3(g). Moreover, the common practice of calibrating using a single bead (rather than averaging as performed in Fig. 3(b)) can result in further loss of accuracy to more distant locations in the FOV.

We also explored axial errors introduced due to axial shift of the phase mask from the conjugate BFP. We observed that these errors, though significantly smaller than the lateral errors, were higher than the achievable precision using DHPSF. Maximum axial errors for $\Delta f = 35$ mm (Fourier plane of the imaged plane) and $\Delta f = 0$ mm (the conjugate BFP) are shown in Fig. 4. Results for $\Delta f = 35$ mm are in agreement with [9], showing similar form of axial error magnitude and gradient across the FOV. By placing the phase mask in the conjugate BFP, these errors are reduced three-fold (Fig. 4(b)). The residual errors can be due to other spatially varying aberrations, non-uniform excitation beam over the sample or fitting errors. Such errors have been discussed in detail in [9].

As evident from the above analysis, for DHPSF, suboptimal positioning of the phase mask (to the first order) results in the loss of accuracy and not precision. As accuracy of a localization is independent of the number of collected photons, our findings are directly applicable to real biological samples involving low number of photons.

7. Conclusion

In this work, we have discussed a spatially varying aberration that afflicts 3D super-resolution localization microscopy techniques utilizing engineered PSFs. The aberration exists when wavefront modifying phase is not added precisely in the back focal plane of the objective. Failure to correct this aberration induces significant systematic error in the accuracy of fluorophore localization. We discussed the origin of this problem through simulations and showed experimental results for the aberrated and the optimized systems. We focused on the DHPSF due to its large depth of field, however the results presented are equally relevant for other PSF engineering methods. We found that correcting this aberration gives highly accurate and precise localizations over a wide FOV, in line with theoretical estimations of precision for the DHPSF.

Funding

This work was funded by the MRC Next Generation Optical Microscopy Initiative (MR/K015850/1), EPSRC (EP/L015455/1, EP/M003663/1), Cambridge Trust and HEC Pakistan. We also thank the Royal Society for the University Research Fellowship of S.F.L. (UF120277).